# Auger-excited Photoluminescence from Gold Nanoflowers

Wouter Koopman,*,† Jan Kutschera,† Felix Stete,† and Matias Bargheer*,†,‡

†*Institut für Physik & Astronomie, Universität Potsdam, Karl-Liebknecht-Str. 24-25, 14476 Potsdam, Germany*

‡*Helmholtz Zentrum Berlin, Albert-Einstein-Str. 15, 12489 Berlin, Germany*

E-mail: wouter.koopman@uni-potsdam.de; bargheer@uni-potsdam.de

Phone: +49 (0)331 977 5723; +49 (0)331 977 4272

**Abstract**

Metal photoluminescence is of great interest as a probe for studying excited charges in plasmonic nanostructures. However, the nature of the emission process is still strongly debated. Here, we employ emission spectroscopy with various excitation wavelengths to investigate the excitation pathway in films of gold nanoflowers. The obtained data provide spectroscopic evidence that the luminescence is dominated by Auger-excited intraband emission from gold nanoflowers. While the excitation spectrum clearly demonstrates absorption by interband transitions, the emission spectra could be unequivocally assigned to intraband recombination. Our conclusion is corroborated by a simulation of the wavelength-dependent inter- and intraband emission, that excludes the interband recombination as a source for the observed emission. These results suggest that Auger excitation is a promising route to generate energetic "hot" electrons with energies substantially above the Fermi level. Exploiting this effect could strongly benefit applications for nano-luminescent probes and the progress of plasmon catalysis.

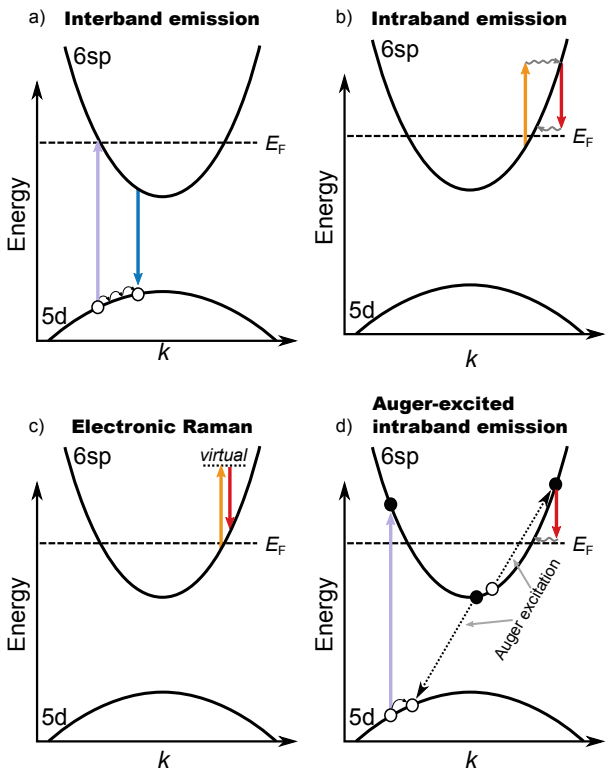


Figure 1: Possible emission processes in metal nanostructures: interband recombination of a *d*-band hole, after exciting an electron to the conduction band (a), intraband excitation and recombination from and to the Fermi level within the conduction band (b), Raman scattering at electrons at the Fermi level (c), intraband recombination after Auger excitation by non-radiative recombination of a *d*-band hole (d)

# Introduction

Photoluminescence (PL) is usually associated with materials possessing an optical band gap, such as molecules and semiconductors. It is less well-known that metals can also exhibit PL, even though the first reports date back more than half a century ago.[1–3] The recent progress in the development of plasmonic metal nanostructures however increasingly draws attention to the topic.[4–8] Emission processes are enhanced by a locally increased photonic mode density in the presence of surface plasmons.[2,5,9] As a consequence, luminescence processes, negligible for bulk metals, become relevant for nanostructures.

Early interest in metal luminescence arose from the desire to remove the spurious background observed in many surface-enhanced Raman (SERS) experiments.[10–15] With increas-

ing insights into emission processes, newer studies also attempt to utilize the light emission from metal nanostructures, e.g. for imaging[16–18] and sensing purposes.[19–21] In particular, in the rapidly growing field of plasmon-assisted chemistry, metal emission is employed as experimental probe to access charge density in plasmonic nanoparticles[22,23] and study charge transfer.[24–27] Its temperature dependence moreover makes it a promising candidate for nano-localized temperature measurements.[28–32]

For the continued development of these applications, a detailed understanding of the emission process in different situations is critical. Despite the growing body of work, a vivid debate surrounds the nature of the emission process. Early works described the high-energy PL from bulk metals by *interband* transitions. Excitation of electrons from the *d*-band leaves behind energetic holes that radiatively recombine with conduction-band electrons[1,2] (Figure 1 a). In nanostructured metals, an additional low-energy, broadband luminescence was frequently reported, that cannot be assigned to interband luminescence. Several authors attribute this emission to surface-assisted recombination of electrons and holes within the conduction band.[4,5,33,34] This *intraband* luminescence requires the presence of a non-thermal charge distribution in the conduction band, often referred to as "hot" electrons[5,8,34,35] (Figure 1 b). An alternative explanation argues that the signal arises from Raman scattering from conduction band electrons, and does not involve an excited charge distribution[15] (Figure 1 c).

In addition to these emission processes, a growing amount of evidence suggests the presence of Auger processes (Figure 1 d). This type of process describes the recombination of electron-hole pairs, where the released energy is transferred non-radiatively to a third charge.[36] Auger recombination is widely studied in semiconductors,[37–40] as a loss-process in light-emitting devices[39,40] and solar cells. In metals, Auger recombination has been proposed for the recombination of a *d*-band hole with a conduction band electron that transfers its energy to another conduction-band electron. Transient two-photon photoemission and luminescence up-conversion measurements indeed suggest that the lifetime of *d*-band holes is

determined by Auger recombination,[36,41,42] limiting the radiative yield of interband recombination processes. Building on this insight, "Auger excitation" of conduction band electrons was proposed to explain an increase in the radiative quantum yield of intraband recombination for the excitation of single gold nanorods in the region of interband absorption.[5] The extent by which Auger processes influence the light emission remained however unclear.

In the present study, we provide evidence that the emission from disordered films of gold nanoflowers (AuNFs) is dominated by the recombination of Auger-excited electrons in the conduction band. AuNF films are well known for their high Raman surface enhancement, but also for their considerable broadband background signal.[31,43] To investigate the luminescence process from absorption to emission, we performed a systematic study on the excitation wavelength dependence of the luminescence. Comparing the emission and excitation spectra to simulations of inter- and intraband emission and absorption revealed a luminescence process in which photons are absorbed by interband transitions and emitted by intraband recombination. We interpret these results as clear evidence for the presence of a highly efficient Auger process that generates excited electrons in the conduction band.

# Results and Discussion

## Emission from gold nanoflower thin-films

The extinction spectrum of the AuNFs in aqueous solution exhibits a broad, but well-defined surface plasmon resonance with a maximum at approximately 550 nm (Figure 2 a, black, dashed line). In contrast, the absorption spectra of the films, obtained with an integrating sphere, did not show a distinguishable plasmon resonance (Figure 2 a, orange line). Instead, a very broad continuous absorption at longer wavelengths resembled the response of a quasi-closed surface.[44] Despite the lack of a distinguishable plasmon resonance on the macro-scale, these films are known to support a strong SERS enhancement[31,43,45] (see also Figure SI3), demonstrating the presence of local hot-spots. Below 480 nm, the increasing absorption is

similar for both the particle and the film and can be assigned to absorption by interband transition.[46,47]

Figure 2 b presents the emission spectrum of the AuNF film for an excitation wavelength of $\lambda_{ex} = 355\,\text{nm}$ (blue line). The emission strongly resembles the plasmon resonance of the AuNFs, as observed in the extinction spectrum of the particles in solution (black, dashed line). This correlation between emission and plasmon resonance was reported for many particles in literature.[4,5,7,9,33,48–50] It is generally interpreted as evidence for Purcell enhanced emission that results from locally increased photonic mode density connected to the plasmon resonance.[7,8] Interestingly, while $\lambda_{ex}$ was well below the onset for interband absorption in this measurement, only a very weak emission was observed at the blue side of the emission spectrum, where one would expect interband emission to occur. Interband emission from the bulk of the film, that was reported by *Mooradian*[1] and *Boyd et al.*,[2] seems to be insignificant in our samples. We thus conclude that the emission spectrum is dominated by the emission from isolated single particles or hot spots.

This observation is distinctly different from earlier studies on the emission of gold nanorods and rough surfaces,[1,2,4,7,38] which reported luminescence from interband recombination in the bulk of the metal at wavelengths below the plasmon resonance. The sole investigation on the luminescence from AuNFs we know of,[49] only reported the emission for wavelengths above 530 nm, for which the reported spectra were comparable to our measurements. The irrelevance of interband emission from the bulk could thus be connected to the particle geometry.

## Integrated emission intensity: excitation processes

A deeper insight into the luminescence process can be obtained by studying the excitation wavelength dependence of the emission spectrum. We recorded emission spectra for different excitation wavelengths ranging from 425 nm, the minimum wavelength achievable with our setup, to 620 nm in intervals of 5 nm (Figure 3 a)). The emission was separated from the

excitation laser by longpass filters with a fixed cut-on wavelength. Because these filters limit the possible excitation wavelength, we used two different filter stets with cut-on wavelengths at 550 nm (window I: excitation: 410 nm to 540 nm, emission: 550 nm to 800 nm) and at 650 nm (window II, excitation: 500 nm to 620 nm, emission: 650 nm to 800 nm), to optimize the trade-off between large spectral emission window and possible excitation wavelength. The excitation power was carefully adjusted before each measurement to obtain the same excitation density.

Most notably, increasing the excitation wavelength decreased the luminescence over the entire spectrum. We would have expected the emission to increase for excitation wavelength in the range of the plasmon resonance, if it originated from the excitation of energetic electrons within the *sp*-band.[7] However, no such behavior was observed. A model study by *Cai et al.*, on the emission quantum yield for four different wavelengths[5] found a decreasing yield for higher excitation wavelengths. They speculated that the involvement of Auger processes might explain this trend. However, no evidence further supporting this claim was presented.

Here, the continuous tunability of our laser allowed us to measure the luminescence for a large number of excitation wavelengths (Figure 3 a). Moreover, by measuring the emission intensity for different excitation wavelengths, we could determine the excitation spectrum related to the emission of our samples (Figure 3 b). To this end, we integrated the emission spectra over all wavelengths for each $\lambda_{ex}$. The consistency between the spectra obtained from both emission windows was ensured as we collected the emission for an excitation wavelength of 525 nm in both spectral windows and adjusted the integrated emission from window II to the emission from window I (see also SI for a detailed procedure).

Different from the absorption spectra in Figure 2, excitation spectra only reveal absorption processes preceding the observed emission signal. Here, we employed excitation spectroscopy to distinguish between the possible excitation pathways of gold nanostructures. Figure 3 b) presents the excitation spectrum obtained from the emission in Figure 3 a).

The excitation in Figure 3 b monotonically decreases with increasing wavelength and does not exhibit any correlation to the plasmon resonance. Such a decreasing absorption towards higher wavelengths is expected for absorption by interband excitation of *d*-band electrons.[2] The excitation spectrum related to the possible processes involving *sp*-band electrons, i.e. intraband absorption and electronic Raman scattering, on the other hand, should follow the plasmon absorption (intraband) or scattering (Raman) spectrum.[7,15] Therefore, the excitation spectrum in Figure 3 b strongly suggests that the observed emission is preceded by interband absorption. Moreover, in the case of electronic Raman scattering, the emission should rapidly decrease away from the Raman laser wavelength. We would therefore expect an additional strong decrease in the emission intensity of lower excitation wavelengths. This is however clearly the case for the observed emission (Figure 3 b). We can therefore exclude with a high degree of certainty electronic Raman scattering as the origin of the emission from our AuNF samples.

To further investigate the absorption process, we compared the excitation spectrum to the interband absorption of gold. Because the pure interband absorption spectrum is difficult to determine experimentally, we employed a well-established method to simulate the interband transitions.[46,47,51,52] In short, the absorption was expressed via the dissipative, imaginary permittivity connected to the interband transitions. Based on Fermis' golden rule for a system with a continuum of states, the imaginary permittivity can be expressed as:[53]

$$\mathrm{Im}(\epsilon(\omega_{abs})) = \frac{4\pi^2 q_e^2}{\epsilon_0 m_e^2 \omega^2} \int A(E_f, E_i)\rho_{Abs}(E_f, E_i) \cdot [f_e(E_i, T) f_h(E_f, T)] dE. \quad (1)$$

Here, $E_i$ and $E_f = E_i + \hbar\omega_{abs}$ are the initial and final states connected by the photon energy $\omega_{abs}$, and $A(E_f, E_i)$ is an oscillator strength comprising the transition dipole moment. The joint density of states (JDOS) for absorption, $\rho_{Abs}(E_i, E_f)$, gives the combined density of *d*-band states with initial energy $E_i$ and *sp*-band states with final energy $E_f$. The electron, $f_e(E_i, T)$, and hole, $f_h(E_f, T) = 1 - f_e(E_f, T)$, distribution functions describe the probability

of finding an electron at the energy $E_i$ and no electron (i.e. a hole) at the energy $E_f$.[52] As the electrons are in thermal equilibrium before the absorption process, $f_e(E,T)$ is given by the Fermi-Dirac distribution for a temperature $T$.

To calculate $\mathrm{Im}(\epsilon(\omega_{abs}))$ at a given frequency $\omega_{abs}$, the integral in Equation 1 must in principle be evaluated over the entire $k$-space. It can however be greatly simplified, as $\rho_{Abs}$ is strongly dominated by contributions from van-Hove singularities at critical points in the band structure.[54] The van Hove singularities relevant to the investigated energy range are located close to the $L$- and $X$-points of the reciprocal lattice (Figure 4 a,b). Their absorption edges are located at energies of approximately 2.2 eV and 1.8 eV. As $F(E_f, E_i)$ varies only marginally around the critical point, it can be viewed as constant and be removed from the integral. The remaining integral was evaluated numerically. Further details on the calculations can be found in the original *Rosei* references.[46,47,55]

Figure 3 b presents a comparison of the experimental excitation spectrum with the simulated imaginary permittivity representing the interband absorption. The experimental data exhibit a remarkable correspondence to the progression obtained from our simulation, up to the form of the characteristic $M1$-type van-Hoove singularity at the $X$-point.[54] From this correspondence, we conclude that the observed emission is preceded by the absorption of photons via interband transition.

Interestingly, the emission spectrum presented in Figure 2 b, did not exhibit emission at the typical interband wavelengths. Moreover, the prominent presence of absorption at the $X$-point is puzzling. Generally, emission at the $X$-point is considered unlikely. Interband emission occurs if a $d$-band hole recombines with an arbitrary conduction band electron. At close the $X$-point the excited hole relaxes towards the symmetry point in $k$-space, where no electrons in the conduction band exist. At the same time the excited electrons relax away from the symmetry point and are subsequently not available for recombination any longer. Thus recombination can only occur for a small energy region, close to the wavelength of the absorption[2] (see also Figure 4 a)). Accordingly, literature does not report interband emission

of gold in the NIR region.[2,5,50] These discrepancies in the experimental observations indicate a complex process for the emission. We propose that the observations can be reconciled, if we assume a very efficient excitation of conduction band electrons by Auger excitation (Figure 1 d).

## Luminescence spectra: recombination mechanism

In the last section, we proposed that the excitation of electrons in the *sp*-band by Auger recombination could explain our seemingly contradictory conclusion obtained from the emission and excitation spectra. In an Auger process, a *d*-band hole recombines with an *sp*-band electron, but instead of releasing its energy by emitting a photon, excess energy and momentum are transferred to another electron in the *sp*-band (Figure 1 d). The energy of the excited electron can be as high as the energy of the hole with respect to the Fermi level. It can thus reach values comparable to those achieved by direct intraband excitation. A fraction of the excited (or "hot") conduction band electrons subsequently relaxes radiatively by surface-assisted recombination with holes at the Fermi level. The luminescence intensity of the process is proportional to the number of photons absorbed by interband transitions, while the emission spectrum resembles plasmon-enhanced intraband luminescence. As it is in direct competition with the radiative recombination, a very efficient non-radiative Auger recombination of *d*-band holes suppresses the interband luminescence.

To clarify whether the recorded emission spectra (Figure 3) indeed originate from intraband recombination, we simulated the excitation wavelength-dependent emission spectra for inter- and intraband recombination processes. In general, the emission originating from the recombination of electrons and holes can be calculated with a procedure similar to the one we used to calculate absorptive transitions in the last section. To simulate the emission, we explicitly calculated Fermis' golden rule for systems with a continuum of states. Different from Equation 1 the initial, $E_i$, and final, $E_f = E_i - \hbar\omega_{em}$, states are now connected via the energy of the emitted photon, $\hbar\omega_{em}$.[2,8] Moreover, the emission also depends on the sur-

rounding photonic mode density, $\rho_{phot}$, which is strongly increased by the plasmon resonance. Therefore the emission rate reads:[8]

$$\Gamma_{em}(\omega_{em}) \propto \rho_{phot}(\omega_{em})|\vec{\mu}|^2 \cdot \int \rho_J(E_i, E_f) f_e(E_i, T) f_h(E_f, T) dE \tag{2}$$

The integral in Equation 2 can once again be limited to the critical $X$- and $L$-points and $\vec{\mu}$ is assumed to be constant. The excitation wavelength dependence of the emission spectrum then originates from the population-weighted joint density of states inside the integral, which strongly differs for intra- and interband recombination. In particular, $f_e$ and $f_h$ become non-equilibrium distributions different from the Fermi-Dirac distribution. We thus need to compare the value of this integral between simulation and experiment.

The prefactors in Equation 2, in particular $\rho_{phot}$, strongly depend on the local environment. As these factors are constant in $\lambda_{ex}$, we canceled their influence by calculating the ratio of the emission for all $\lambda_{ex}$ to the emission spectrum excited at $\lambda_{ex} = 425\,\mathrm{nm}$:

$$\frac{I}{I_{425}} = \frac{I_{em}(\lambda_{ex} > 425)}{I_{em}(\lambda_{ex} = 425)} \tag{3}$$

The resulting spectrum is a measure of the change in the population-weighted JDOS that can be readily accessed both by experiment and simulation.

Figure 5 b) presents $I/I_{425}$ for all $\lambda_{ex}$ measured in window I. For all $\lambda_{ex}$ the amplitude remains below one, reflecting the decreasing intensity of the emission, and the spectrum is characterized by a slowly varying, flat progression. The weak minimum around $\lambda_{em} < 560\,\mathrm{nm}$ becomes more pronounced for higher $\lambda_{ex}$. To clarify the emission mechanism, we compared the $I/I_{425}$ spectrum to simulations of interband and intraband emission.

We simulated the interband emission employing a model introduced by *Boyd et al.*[2] In short, it assumes that the electrons that are excited to the *sp*-band and the holes remaining in the *d*-band can relax within their respective band before they recombine. This leads to distributions, for both electrons ($f_e(E)$) and holes ($f_h(E)$) that exponentially decay away

from the initial excitation energy (see Figure 4 c). For electrons it reads:

$$f_e(E) = f^T(E,T) + \Theta(E - E_0)\exp\frac{E - E_0}{\gamma_e} - \Theta(E_{h,0} - E_h)\exp\frac{E_{h,0} - E_h}{\gamma_h} \tag{4}$$

and accordingly for holes:

$$f_h(E_h) = 1 - f^T(E_h,T) + \Theta(E_{h,0} - E_h)\exp\frac{E_{h,0} - E_h}{\gamma_h} - \Theta(E - E_0)\exp\frac{E - E_0}{\gamma_e} \tag{5}$$

Here, $f^T(E,T)$ denotes the Fermi-Dirac distribution, $\Theta(E)$ the Heaviside function, $E_0$ the initial energy of the excited electrons,$E_{h,0} = E_0 - \hbar\omega_{abs}$ the initial energy of the excited holes and $E_h = E - \hbar\omega_{em}$ the energy of emission. The parameters $\gamma_e$ and $\gamma_h$ are adjustable exponential widths, representing the relaxation of electrons and holes before recombination. We used a rough estimate of about 80 meV, obtained from the lifetime of $d$-band holes of $\tau_h < 50$ fs.[36,42]

Using these charge distributions, we calculated the emission rate via Equation 2, where $\rho_J(\omega_{em})$ is identical to the JDOS determined for the absorption process, only now we use the energy of the emitted photons $\hbar\omega_{em}$ instead of $\hbar\omega_{ex}$. Finally, we obtained the emission spectrum taking into account the changing absorption for the different $\omega_{ex}$ as:

$$I(\omega_e x) \propto A(\omega_{ex}) \cdot \Gamma_{em}(\omega_{em}). \tag{6}$$

The factors $A(\omega_{ex})$ describe the change in the absorption relative to the absorption at $\lambda_{ex} = 425$ nm, as determined from the excitation spectrum in Figure 3. The only variable factors in this calculation are $\gamma_e$ and $\gamma_h$.

The simulated $I/I_{425}$ spectra for interband recombination are presented in Figure 5 a). Most notably, for large $\lambda_{ex}$ the maximum of $I/I_{425}$ increases significantly above one, even though the relative absorption $A(\omega_{ex})$ decreases. This behavior can be rationalized taking into account the progression of the emission spectrum for interband recombination. Inter-

band emission decreases exponentially away from the excitation wavelength.[2,5] Thus, as $\lambda_{ex}$ approaches the cut-on wavelength of the filter, the emission spectrum increasingly shifts into the observation window and a larger fraction of the emission can be observed. A second remarkable feature of the $I/I_{425}$ spectra is the sharp drop above 600 nm. This observation reflects the empty *sp*-band at the $X$-point (Figure 4 a), which prevents emission at energies below the onset of the interband absorption. The simulated interband emissions differ strongly from the $I/I_{425}$ spectra calculated from the experimental data. This confirms the conclusion already drawn from the emission spectrum in Figure 2: the observed luminescence does not originate from interband recombination.

Contrary to interband recombination, intraband recombination violates momentum conservation unless the missing momentum is provided by scattering at phonons or the surface of a nanostructure.[7,56,57] As a result, $\rho_J(E_i, E_f)$ in Equation 2 can be assumed to be approximately constant in $\omega_{ex}$.[8,58] The form of the non-equilibrium electron and hole distributions has been extensively discussed in literature by several groups. Most authors agree on a flat distribution of excited electrons and holes, directly above and below the Fermi level as depicted in Figure 4. Here, we applied the analytical formulation proposed by *Dubi & Sivan*:[8]

$$f(E) = f^T(E,T) + \Delta f_e^{NT}(E) - \Delta f_h^{NT}, \tag{7}$$

$$\Delta f_e^{NT}(E) = \delta_E(E,T)\left[(1 - f^T(E,T)) \cdot f^T(E - \hbar\omega_{ex}, T)\right], \tag{8}$$

$$\Delta f_h^{NT}(E) = \delta_E(E,T)\left[f^T(E,T) \cdot (1 - f^T(E + \hbar\omega_{ex}, T)\right]. \tag{9}$$

The non-equilibrium terms $\Delta f_e^{NT}(E)$ and $\Delta f_h^{NT}(E)$ represent the excited distribution of electrons and holes. They correspond to thermally smeared-out step functions, whose energy width is given by the excitation energy. The parameter $\delta_E$ represents the strength of the

population inversion (Figure 4) and is determined by the ratio of the excitation and decay rates.[8] As in particular the former depends on the absorbed light intensity, we assumed that $\delta_E(\omega_{ex}) = \zeta A(\omega_{ex})$. The proportionality constant, $\zeta$, presents the sole fudging factor in the model and was assumed to be identical for all $\omega_{ex}$.

The simulated $I/I_{425}$ spectra (Figure 5 c)) reproduce the general behavior of the experimental spectra (Figure 5 b)) surprisingly well. In particular, the flat behavior and the gradual decrease for higher wavelengths are accurately described. The broadband emission originates from the broad non-equilibrium charge distribution above and below the $E_F$ while the gradual decrease towards lower wavelengths reflects its cut-off of the electron distribution at the excitation energy (Figure 4 d). The lower the excitation energy, the further the cut-off shifts to higher wavelengths. We achieved the best agreement between experiment and data for $\zeta = 1 \times 10^{-2}$ and resulting values for $\delta_E(\omega_{ex})$ between $2 \times 10^{-3}$ and $10^{-2}$. This population inversion is considerably larger than the inversion estimated for direct intraband excitation of around $\delta_E \approx 10^{-3}$ - $10^{-9}$ as predicted by *Dubi & Sivan*[58] for an 2.6× lower excitation intensity.

The most notable deviation between experiment and simulation is a minimum between 550 nm and 560 nm in the experimental data the simulation could not reproduce. At this wavelength, emission by interband transitions is expected. Hence, we attribute this deviation to the presence of a weak additional interband recombination process.

The comparison between simulation and experimental data clearly confirms surface-assisted intraband recombination as the origin of the observed luminescence. Thus, we conclude that the most likely explanation for the luminescence observed from AuNF films is indeed the recombination of charges within the conduction band that were excited by an efficient Auger process. This interpretation is supported by several transient measurements that cite Auger recombination as the lifetime-limiting process for *d*-band holes in gold,[36,42] and hence indicate that Auger recombination is more efficient than radiative interband recombination. This also confirms speculations about the increase in quantum yield of interband

luminescence by Auger processes.[7] Why the Auger recombination process in the investigated AuNF films is seemingly more efficient than in other nanostructures, up to a degree where it fully suppresses bulk-interband recombination, remains unclear and should be the subject of further investigations.

Finally, we want to note that in our opinion Auger excitation might also be of importance for plasmon-driven photocatalysis. For example, the group of *Baldi* observed an isotropic growth of a silver shell around a gold nanorod if the particle was illuminated at a wavelength overlapping with the interband transitions while no growth was observed for excitation at the longitudinal resonance of the rod at energies below the interband onset.[59] The observed growth however requires the presence of energetic electrons. These are not provided in an interband transition but might be generated by Auger excitation. As our simulations indicate that the population inversion in our samples is higher than expected from direct intraband excitation, Auger excitation could be a feasible route to enhance the generation of "hot" electrons.

# Conclusions

In this article, we investigated the origin of the strong luminescence from disordered films of gold nanoflowers. To this end, we studied the excitation wavelength dependence of the emission spectrum for excitation wavelengths from $\lambda_{ex} = 425\,\mathrm{nm}$ to $630\,\mathrm{nm}$. The strong correlation of the excitation spectrum extracted from this data with the interband absorption of gold demonstrated that the emission is preceded by the excitation of an electron from the *5d*-band above the Fermi level. On the other hand, the spectral evaluation of the luminescence with varying excitation wavelengths could only be explained by intraband recombination within the conduction band as it could not be brought into agreement with simulations of interband luminescence. We explain these observations with the presence of an efficient Auger scattering process that produces an excited charge distribution in the

conduction band by recombination of $d$-band holes.

These results shed new light on the debate on metal-luminescence. On the one hand, because the emission involves a real state, we can also exclude the involvement of an electronic Raman scattering with a high degree of certainty. Moreover, the selection of an excitation wavelength alone is not sufficient to conclude the presence or absence of interband luminescence. Finally, in the investigated samples, the Auger excitation process is more efficient than interband recombination or direct intraband excitation of "hot" electrons. It is unclear if this result can be generalized. However, it might potentially show a route to generate energetic charges above the Fermi level more efficiently and hence could be of great interest for luminescence or photostatic applications involving metal nanostructures.

# Methods

## Sample Preparation

We prepared thin films of gold nanoflowers (AuNF) according to a previously reported wet-chemical method using a HEPES buffer solution as a structure-directing agent.[43] Initially, 200 µL of 100 mM of HEPES buffer solution (pH $7.4 \pm 0.5$) were thoroughly mixed with 1.8 mL water for 5 min. Subsequently, 40 µL of 25 mM $HAuCl_4$(aq) solution were quickly added and the mixture was aged undisturbed for 2 h. The color change from pale yellow via colorless to dark blue confirmed the growth process. The final AuNFs were centrifuged and washed three times by re-dispersion in 500 µL water. Transmission electron-beam microscopy (TEM) showed that the resulting particles resemble spheres with a diameter of $(60 \pm 5)$ nm and an irregular surface with sharp edges (see Figure SI1).

Disordered films were prepared by drop-casting AuNFs onto Si substrates and drying the samples for at least 3 h at room temperature. The latter were previously cleaned first by 30 min UV-ozone plasma cleaning and subsequently by washing in ethanol and water. The films show a high particle density with no regular structure (Figure SI2). After drop-casting,

we cleaned the samples of any residuals by 60 min UV-ozone plasma cleaning. Previous experiments demonstrated a strong surface enhancement for Raman scattering (SERS) on these types of samples, pointing to the presence of regions with high field enhancements.[31,43,45] Raman measurements on the cleaned samples did not show signs of remaining contaminants.

### Emission and Excitation Spectroscopy

Emission and excitation spectroscopy was performed using a home-built micro-spectrometer. The samples were excited by a laser through a 60x objective (Nikon 60x Plan Fluor ELWD, N.A. = 0.75) and the emission was collected in a reflection geometry through the same objective. Excitation and emission were separated by a filter assembly (dichroic beamsplitter, plus emission and excitation filters). The characteristics of the filter were chosen according to the excitation wavelength. We used filter sets with cut-off wavelengths of 550 nm and 650 nm. The collected luminescence was detected by an EMCCD camera (Andor Newton) behind a grating spectrograph (Andro Kymera 328i). For tunable visible excitation we utilized a supercontinuum laser (NKT SuperK EXTREME) coupled to a monochromator (NKT SuerpK Varia). The excitation power was fixed to 16 kW cm$^{-2}$ (0.5 mW @ 2 µm spot size) for all measurements and the spectral bandwidth was 10 nm. UV-excitation at $\lambda_{ex} = 355$ nm was performed with a separate cw-laser (Coherent GENESIS-355-150) adjusted to the same excitation power.

## Acknowledgements

The authors acknowledge funding by the Deutsche Forschungsgemeinschaft (DFG, German Research Foundation) – CRC/SFB 1636 – Project ID 510943930 - Project No. A01/A04/Z02

# References

# References

(1) Mooradian, A. Photoluminescence of Metals. *Phys. Rev. Lett.* **1969**, *22*, 185–187.

(2) Boyd, G. T.; Yu, Z. H.; Shen, Y. R. Photoinduced luminescence from the noble metals and its enhancement on roughened surfaces. *Phys. Rev. B* **1986**, *33*, 7923–7936.

(3) Apell, P.; Monreal, R.; Lundqvist, S. Photoluminescence of noble metals. *Phys. Scr.* **1988**, *38*, 174.

(4) Beversluis, M. R.; Bouhelier, A.; Novotny, L. Continuum generation from single gold nanostructures through near-field mediated intraband transitions. *Phys. Rev. B* **2003**, *68*, 115433.

(5) Cai, Y.-Y.; Liu, J. G.; Tauzin, L. J.; Huang, D.; Sung, E.; Zhang, H.; Joplin, A.; Chang, W.-S.; Nordlander, P.; Link, S. Photoluminescence of Gold Nanorods: Purcell Effect Enhanced Emission from Hot Carriers. *ACS Nano* **2018**, *12*, 976–985.

(6) Tauzin, L. J.; Cai, Y.-y.; Smith, K. W.; Hosseini Jebeli, S. A.; Bhattacharjee, U.; Chang, W.-S.; Link, S. Exploring the Relationship between Plasmon Damping and Luminescence in Lithographically Prepared Gold Nanorods. *ACS Photonics* **2018**, *5*, 3541–3549.

(7) Cai, Y.-Y.; Tauzin, L. J.; Ostovar, B.; Lee, S.; Link, S. Light emission from plasmonic nanostructures. *J. Chem. Phys.* **2021**, *155*, 060901.

(8) Sivan, Y.; Dubi, Y. Theory of "Hot" Photoluminescence from Drude Metals. *ACS Nano* **2021**, *15*, 8724–8732.

(9) Hu, H.; Duan, H.; Yang, J. K. W.; Shen, Z. X. Plasmon-Modulated Photoluminescence of Individual Gold Nanostructures. *ACS Nano* **2012**, *6*, 10147–10155.

(10) Furtak, T. E.; Reyes, J. A Critical Analysis of Theoretical Models for the Giant Raman Effect from Adsorbed Molecules. *Surf. Sci.* **1980**, *93*, 351–382.

(11) Otto, A.; Mrozek, I.; Grabhorn, H.; Akemann, W. Surface-Enhanced Raman Scattering. *J. Phys.: Condens.Matter* **1992**, *4*, 1143.

(12) Kneipp, K.; Wang, Y.; Kneipp, H.; Perelman, L. T.; Itzkan, I.; Dasari, R. R.; Feld, M. S. Single Molecule Detection Using Surface-Enhanced Raman Scattering (SERS). *Phys. Rev. Lett.* **1997**, *78*, 1667–1670.

(13) Moskovits, M. Surface-Enhanced Raman Spectroscopy: A Brief Retrospective. *J. Raman Spectrosc.* **2005**, *36*, 485–496.

(14) Mahajan, S.; Cole, R. M.; Speed, J. D.; Pelfrey, S. H.; Russell, A. E.; Bartlett, P. N.; Barnett, S. M.; Baumberg, J. J. Understanding the Surface-Enhanced Raman Spectroscopy "Background". *J. Phys. Chem. C* **2010**, *114*, 7242–7250.

(15) Hugall, J. T.; Baumberg, J. J. Demonstrating Photoluminescence from Au Is Electronic Inelastic Light Scattering of a Plasmonic Metal: The Origin of SERS Backgrounds. *Nano Lett.* **2015**, *15*, 2600–2604.

(16) Jiang, Y.; Horimoto, N. N.; Imura, K.; Okamoto, H.; Matsui, K.; Shigemoto, R. Bioimaging with Two-Photon-Induced Luminescence from Triangular Nanoplates and Nanoparticle Aggregates of Gold. *Adv. Mater.* **2009**, *21*, 2309–2313.

(17) Titus, E. J.; Willets, K. A. Accuracy of Superlocalization Imaging Using Gaussian and Dipole Emission Point-Spread Functions for Modeling Gold Nanorod Luminescence. *ACS Nano* **2013**, *7*, 6258–6267.

(18) Wilson, A. J.; Devasia, D.; Jain, P. K. Nanoscale optical imaging in chemistry. *Chem. Soc. Rev.* **2020**, *49*, 6087–6112.

(19) Lu, G.; Hou, L.; Zhang, T.; Liu, J.; Shen, H.; Luo, C.; Gong, Q. Plasmonic Sensing via Photoluminescence of Individual Gold Nanorod. *J. Phys. Chem. C* **2012**, *116*, 25509–25516.

(20) Zhang, B.; Lan, T.; Huang, X.; Dong, C.; Ren, J. Sensitive Single Particle Method for Characterizing Rapid Rotational and Translational Diffusion and Aspect Ratio of Anisotropic Nanoparticles and Its Application in Immunoassays. *Anal. Chem.* **2013**, *85*, 9433–9438.

(21) Hauler, O.; Jakob, L. A.; Braun, K.; Laible, F.; Fleischer, M.; Meixner, A. J.; Wackenhut, F. Sensitive Interferometric Plasmon Ruler Based on a Single Nanodimer. *J. Phys. Chem. C* **2021**, *125*, 6486–6493.

(22) Sundararaman, R.; Narang, P.; Jermyn, A. S.; Goddard III, W. A.; Atwater, H. A. Theoretical Predictions for Hot-Carrier Generation from Surface Plasmon Decay. *Nat. Commun.* **2014**, *5*, 5788.

(23) Searles, E. K.; Gomez, E.; Lee, S.; Ostovar, B.; Link, S.; Landes, C. F. Single-Particle Photoluminescence and Dark-Field Scattering during Charge Density Tuning. *J. Phys. Chem. Lett.* **2023**, *14*, 318–325.

(24) Zheng, Z.; Majima, T. Nanoplasmonic Photoluminescence Spectroscopy at Single-Particle Level: Sensing for Ethanol Oxidation. *Angew. Chem., Int. Ed.* **2016**, *55*, 2879–2883.

(25) Shahine, I.; Jradi, S.; Beydoun, N.; Gaumet, J.-J.; Akil, S. Plasmon-Enhanced Photoluminescence and Photocatalysis Reactions in Metal-Semiconductor Nanomaterials: UV-Generated Hot Electron in Gold-Zinc Oxide. *ChemPhotoChem* **2020**, *4*, 181–194.

(26) Lee, S. A.; Link, S. Chemical Interface Damping of Surface Plasmon Resonances. *Acc. Chem. Res.* **2021**, *54*, 1950–1960.

(27) Lee, S. A.; Ostovar, B.; Landes, C. F.; Link, S. Spectroscopic Signatures of Plasmon-Induced Charge Transfer in Gold Nanorods. *J. Chem. Phys.* **2022**, *156*, 064702.

(28) Huang, J.; Wang, W.; Murphy, C. J.; Cahill, D. G. Resonant Secondary Light Emission from Plasmonic Au Nanostructures at High Electron Temperatures Created by Pulsed-Laser Excitation. *Proc. Natl. Acad. Sci. U. S. A.* **2014**, *111*, 906–911.

(29) Xie, X.; Cahill, D. G. Thermometry of Plasmonic Nanostructures by Anti-Stokes Electronic Raman Scattering. *Appl. Phys. Lett.* **2016**, *109*, 183104.

(30) Carattino, A.; Caldarola, M.; Orrit, M. Gold Nanoparticles as Absolute Nanothermometers. *Nano Lett.* **2018**, *18*, 874–880.

(31) Koopman, W.; Sarhan, R. M.; Stete, F.; Schmitt, C. N. Z.; Bargheer, M. Decoding the kinetic limitations of plasmon catalysis: the case of 4-nitrothiophenol dimerization. *Nanoscale* **2020**, *12*, 24411–24418.

(32) Baffou, G. Anti-Stokes Thermometry in Nanoplasmonics. *ACS Nano* **2021**, *15*, 5785–5792.

(33) Fang, Y.; Chang, W.-S.; Willingham, B.; Swanglap, P.; Dominguez-Medina, S.; Link, S. Plasmon Emission Quantum Yield of Single Gold Nanorods as a Function of Aspect Ratio. *ACS Nano* **2012**, *6*, 7177–7184.

(34) Haug, T.; Klemm, P.; Bange, S.; Lupton, J. M. Hot-Electron Intraband Luminescence from Single Hot Spots in Noble-Metal Nanoparticle Films. *Phys. Rev. Lett.* **2015**, *115*, 067403.

(35) Cai, Y.-Y.; Sung, E.; Zhang, R.; Tauzin, L. J.; Liu, J. G.; Ostovar, B.; Zhang, Y.; Chang, W.-S.; Nordlander, P.; Link, S. Anti-Stokes Emission from Hot Carriers in Gold Nanorods. *Nano Lett.* **2019**, *19*, 1067–1073.

(36) Bauer, M.; Marienfeld, A.; Aeschlimann, M. Hot electron lifetimes in metals probed by time-resolved two-photon photoemission. *Prog. Surf. Sci.* **2015**, *90*, 319–376.

(37) Das, A.; Al-Jishi, R. Theory of Interband Auger Recombination in Semiconductors. *Phys. Rev. B* **1990**, *41*, 3551–3560.

(38) Gao, Y.; Sandeep, C. S. S.; Schins, J. M.; Houtepen, A. J.; Siebbeles, L. D. A. Disorder strongly enhances Auger recombination in conductive quantum-dot solids. *Nat. Commun.* **2013**, *4*, 2329.

(39) Klimov, V. I.; Mikhailovsky, A. A.; Xu, S.; Malko, A.; Hollingsworth, J. A.; Leatherdale, C. A.; Eisler, H.-J.; Bawendi, M. G. Optical Gain and Stimulated Emission in Nanocrystal Quantum Dots. *Science* **2000**, *290*, 314–317.

(40) Zhou, Y.; Califano, M. Decoupling Radiative and Auger Processes in Semiconductor Nanocrystals by Shape Engineering. *J. Phys. Chem. Lett.* **2021**, *12*, 9155–9161.

(41) Knoesel, E.; Hotzel, A.; Wolf, M. Ultrafast dynamics of hot electrons and holes in copper: Excitation, energy relaxation, and transport effects. *Phys. Rev. B* **1998**, *57*, 12812–12824.

(42) Lee, S. A.; Kuhs, C. T.; Searles, E. K.; Everitt, H. O.; Landes, C. F.; Link, S. d-Band Hole Dynamics in Gold Nanoparticles Measured with Time-Resolved Emission Upconversion Microscopy. *Nano Lett.* **2023**, *23*, 3501–3506.

(43) Sarhan, R. M.; Koopman, W.; Schuetz, R.; Schmid, T.; Liebig, F.; Koetz, J.; Bargheer, M. The importance of plasmonic heating for the plasmon-driven photodimerization of 4-nitrothiophenol. *Sci. Rep.* **2019**, *9*, 3060.

(44) Kossoy, A.; Merk, V.; Simakov, D.; Leosson, K.; Kéna-Cohen, S.; Maier, S. A. Optical and Structural Properties of Ultra-thin Gold Films. *Adv. Opt. Mater.* **2015**, *3*, 71–77.

(45) Koopman, W.; Titov, E.; Sarhan, R. M.; Gaebel, T.; Schürmann, R.; Mostafa, A.; Kogikoski Jr., S.; Milosavljević, A. R.; Stete, F.; Liebig, F.; Schmitt, C. N.; Koetz, J.; Bald, I.; Saalfrank, P.; Bargheer, M. The Role of Structural Flexibility in Plasmon-Driven Coupling Reactions: Kinetic Limitations in the Dimerization of Nitro-Benzenes. *Adv. Mater. Interfaces* **2021**, *8*, 2101344.

(46) Guerrisi, M.; Rosei, R.; Winsemius, P. Splitting of the interband absorption edge in Au. *Phys. Rev. B* **1975**, *12*, 557–563.

(47) Rosei, R. Temperature modulation of the optical transitions involving the Fermi surface in Ag: Theory. *Phys. Rev. B* **1974**, *10*, 474–483.

(48) Yorulmaz, M.; Khatua, S.; Zijlstra, P.; Gaiduk, A.; Orrit, M. Luminescence Quantum Yield of Single Gold Nanorods. *Nano Lett.* **2012**, *12*, 4385–4391.

(49) Zhang, T.; Lu, G.; Shen, H.; Shi, K.; Jiang, Y.; Xu, D.; Gong, Q. Photoluminescence of a single complex plasmonic nanoparticle. *Sci. Rep.* **2014**, *4*, 3867.

(50) Ostovar, B.; Cai, Y.-Y.; Tauzin, L. J.; Lee, S. A.; Ahmadivand, A.; Zhang, R.; Nordlander, P.; Link, S. Increased Intraband Transitions in Smaller Gold Nanorods Enhance Light Emission. *ACS Nano* **2020**, *14*, 15757–15765.

(51) Stoll, T.; Maioli, P.; Crut, A.; Del Fatti, N.; Vallée, F. Advances in femto-nano-optics: ultrafast nonlinearity of metal nanoparticles. *Eur. Phys. J. B* **2014**, *87*, 260.

(52) Stete, F.; Bargheer, M.; Koopman, W. Ultrafast dynamics in plasmon–exciton core–shell systems: the role of heat. *Nanoscale* **2023**, *15*, 16307–16313.

(53) Dresselhaus, M. S.; Dresselhaus, G.; Cronin, S. B.; Gomes Souza Filho, A.; Filho, A. G. S. *Solid state properties: from bulk to nano*; Graduate texts in physics; Springer: Berlin, 2018.

(54) Yu, P. Y.; Cardona, M. *Fundamentals of Semiconductors: Physics and Materials Properties*; Graduate Texts in Physics; Springer Berlin Heidelberg Springer e-books Imprint: Springer: Berlin, Heidelberg, 2010.

(55) Antonangeli, F.; Colavita, E.; Rosei, R.; Salusti, S. E. Optical gaps and interband matrix elements of silver as a function of temperature. *Nuov Cim B* **1974**, *24*, 121–129.

(56) Maruyama, Y.; Futamata, M. Inelastic Scattering and Emission Correlated with Enormous SERS of Dye Adsorbed on Ag Nanoparticles. *Chem. Phys. Lett.* **2005**, *412*, 65–70.

(57) Bayle, M.; Combe, N.; Sangeetha, N. M.; Viau, G.; Carles, R. Vibrational and Electronic Excitations in Gold Nanocrystals. *Nanoscale* **2014**, *6*, 9157–9165.

(58) Sivan, Y.; Un, I. W.; Dubi, Y. Assistance of metal nanoparticles in photocatalysis - nothing more than a classical heat source. *Faraday Discuss.* **2019**, *214*, 215–233.

(59) Kamarudheen, R.; Aalbers, G. J. W.; Hamans, R. F.; Kamp, L. P. J.; Baldi, A. Distinguishing Among All Possible Activation Mechanisms of a Plasmon-Driven Chemical Reaction. *ACS Energy Lett.* **2020**, *5*, 2605–2613.

## Author Contributions

W.K. and J.K. conducted the experiments and evaluated the data. W.K. wrote the manuscript with the support of all authors. F.S. contributed to the data interpretation and provided the figures and graphical design. M.B. supervised the work and worked on the manuscript.

## Competing Interests

The authors declare no competing interests.

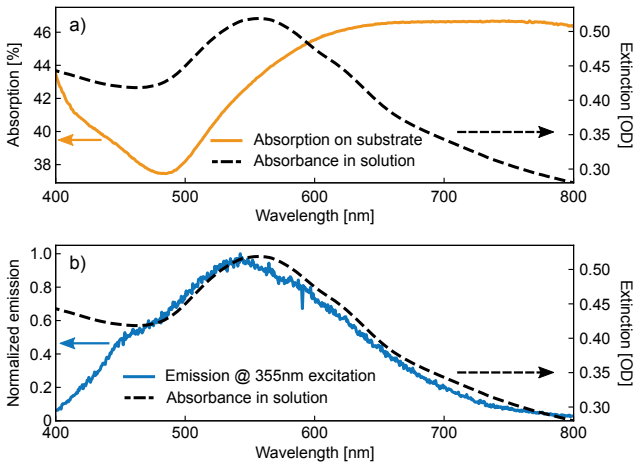


Figure 2: (a) The extinction of the AuNFs in aqueous solution (dashed line) exhibits a pronounced plasmon resonance, while the absorption of the AuNF film (orange line) shows a very broad absorption feature. (b) The emission of the AuNF films excited at $\lambda_{ex} = 355\,\text{nm}$ (blue line) closely resembles the plasmon resonance in solution (dashed line).

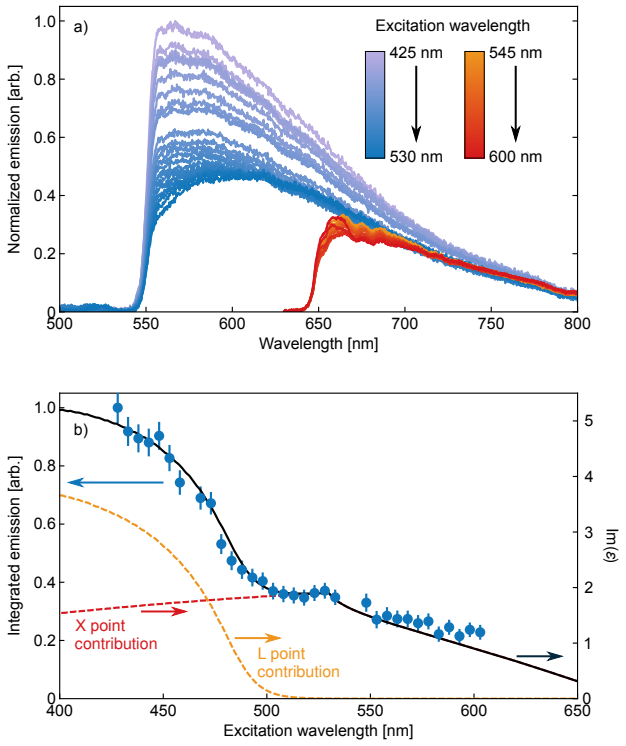


Figure 3: (a) Excitation wavelength-dependent emission spectra with longpass filters at 550 nm (window I - blue lines) and 650 nm (window II - red lines). Darker colors represent longer excitation wavelengths. The intensity of the spectra in window II were adjusted to the spectra in window I. (b) Excitation spectrum of the AuNF film calculated from (a) (blue points). The excitation measurements closely follow the simulated interband absorption spectrum at the $L$- and $X$-points (orange and red dashed lines).

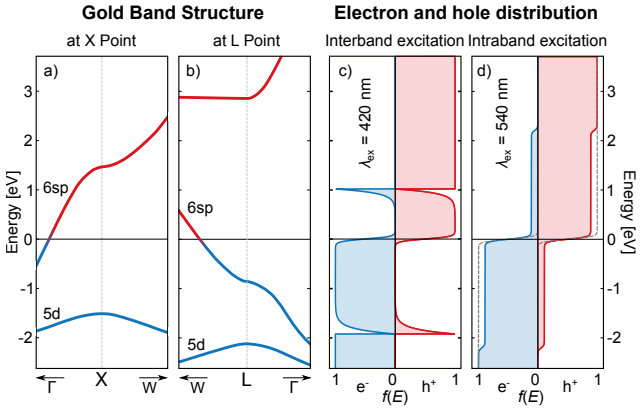


Figure 4: The band structure of gold at optically relevant regions close to the $X$- and $L$-point (a,b). The excited charge distributions used in the simulations of interband (c) and intraband (d) luminescence, as proposed by Boyd and Sivan & Dubi.

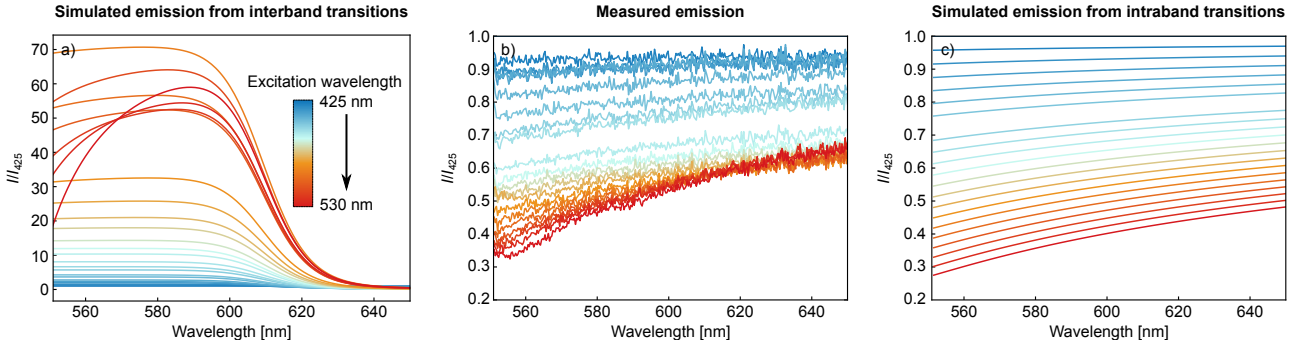


Figure 5: The simulated $I/I_{425}$ emission spectrum for interband emission (a) differs strongly from the measured spectrum (b), while the emission simulated for intraband emission reproduces the experimental spectrum rather well (c). The spectra were determined for excitation wavelength from $\lambda_{ex} = 430\,\text{nm}$ to $550\,\text{nm}$.